Published in final edited form as:
IEEE Trans Med Imaging. 2012 December ; 31(12): 2335–2342. doi:10.1109/TMI.2012.2217979.

Relaxation in X-Space Magnetic Particle Imaging

Laura R. Croft,
Department of Bioengineering, University of California, Berkeley, CA 94720 USA (lcroft@berkeley.edu)

Patrick W. Goodwill, and
Department of Bioengineering, University of California, Berkeley, CA 94720 USA

Steven M. Conolly
Departments of Bioengineering and Electrical Engineering and Computer Sciences, University of California, Berkeley, CA 94720 USA

Abstract

Magnetic particle imaging (MPI) is a new imaging modality that noninvasively images the spatial distribution of superparamagnetic iron oxide nanoparticles (SPIOs). MPI has demonstrated high contrast and zero attenuation with depth, and MPI promises superior safety compared to current angiography methods, X-ray, computed tomography, and magnetic resonance imaging angiography. Nanoparticle relaxation can delay the SPIO magnetization, and in this work we investigate the open problem of the role relaxation plays in MPI scanning and its effect on the image. We begin by amending the x-space theory of MPI to include nanoparticle relaxation effects. We then validate the amended theory with experiments from a Berkeley x-space relaxometer and a Berkeley x-space projection MPI scanner. Our theory and experimental data indicate that relaxation reduces SNR and asymmetrically blurs the image in the scanning direction. While relaxation effects can have deleterious effects on the MPI scan, we show theoretically and experimentally that x-space reconstruction remains robust in the presence of relaxation. Furthermore, the role of relaxation in x-space theory provides guidance as we develop methods to minimize relaxation-induced blurring. This will be an important future area of research for the MPI community.

Keywords

Ferrofluid relaxation; ferrohydrodynamics; magnetic nanoparticles; magnetic particle imaging (MPI); relaxation

I. Introduction

Magnetic particle imaging (MPI) is an emerging imaging technology that shows great promise as a safer angiography alternative, particularly for patients with chronic kidney disease (CKD) who represent 25% of patients who present to the angiography suite, and 47% of patients in the USA over the age of 70 [1]–[3]. MPI has no ionizing radiation, and the superparamagnetic iron oxide nanoparticle (SPIO) contrast agent is metabolized directly by the liver rather than by the kidneys [4], [5]. There is ample evidence in the literature that patients with CKD will tolerate SPIO contrast agents far better than iodine or gadolinium [6]. In fact, an SPIO agent (Ferumoxytol, AMAG Pharmaceuticals, Lexington, MA) is

Correspondence to: Laura R. Croft.

approved by the Food and Drug Administration to treat a common complication of CKD, iron deficiency anemia [7].

MPI directly measures the location and concentration of SPIOs. A strong magnetic gradient (~2.3 T/m) creates a field-free-point (FFP), and a time-varying homogeneous field scans the FFP across a region. We can also scan using a field-free-line (FFL), which we use in the projection MPI scanner in this study [8].The variation of the homogeneous excitation field causes SPIOs at the instantaneous FFP or FFL to "flip," and thereby induce a signal in the receive coil. MPI receives no signal from the background tissue, providing for excellent contrast.

The contrast, sensitivity, and safety of MPI are competitive with existing technologies, but MPI currently lags in spatial resolution. MPI systems theory is essential to understand how to optimize spatial resolution along with signal-to-noise ratio (SNR), contrast, hardware and safety concerns. Many studies have made progress in modeling MPI in the temporal harmonic domain and reconstructing with what is known as a *system matrix* [9], [10]. However, reconstruction with a *system matrix* requires multiplying by the inverse of a large system matrix, which may be too complex for real-time reconstruction. The newer x-space analysis views MPI as a scanning process in the image domain [11], [12]. X-space reconstruction has demonstrated linearity and shift-invariance with essentially zero noise gain. Moreover, x-space reconstruction shows promise for realtime reconstruction since it requires only a point-division by the FFP velocity [8], [11]–[13].

Both MPI system theories were derived under an *adiabatic* assumption that SPIO magnetization instantaneously follows an applied magnetic field. This applied field creates a torque on the magnetic dipole moments of the SPIOs and induces the SPIO alignment with that field. However, the orientation of the SPIO dipole moments are also influenced by thermal fluctuations, which promote random rotations, and by the physical barriers that hinder rotation such as viscous resistance. The competition of these torques causes a phenomenon known as relaxation, which delays the magnetization response of SPIOs and is typically described by a first-order Debye relaxation process [14], [15]. Relaxation descriptions for particle magnetization have been studied in ferrofluid literature [15]–[21], primarily for Néel and Brownian relaxation time constants, which are based on thermal processes. Based on this literature, comprehensive models of non-adiabatic MPI magnetization have been derived [22]. Studies indicate relaxation properties of SPIOs may diminish MPI signal [23], [24], but, to date, relaxation artifacts on the reconstructed MPI scans have not been analyzed thoroughly.

In this work, we amend the 1-D x-space theory to account for non-adiabatic SPIO magnetization. We show that the inclusion of relaxation effects is essential for theoretical predications to agree with experimental MPI data. We demonstrate theoretically and experimentally how relaxation blurs the x-space image and deteriorates resolution and SNR in the scanning direction. In a broader context, a simple model of relaxation will enable us to understand how to design MPI scanning to minimize blurring from relaxation and to achieve a desirable image resolution and signal strength. A better understanding of relaxation effects will benefit *both* x-space and harmonic reconstruction methods.

II. Theory

A. Review of Adiabatic X-Space Theory in One Dimension

The x-space theory characterizes MPI as a scanning process in the image domain [11], [12]. Here, we review the 1-D case; for the 3-D case, please see [12]. Under the adiabatic

assumption that relaxation effects are negligible, the scalar magnetization of a SPIO in response to an applied field $H(x, t)$ [A/m] obeys the Langevin equation for paramagnetism

$$M_{\text{adiab}}(x,t)=m\rho(x)\delta(y)\delta(z)\mathcal{L}\left[\frac{H(x,t)}{H_{\text{sat}}}\right] \quad (1)$$

where m [A · m^2] is the magnetic moment of the SPIOs, $\rho(x)$ [particles/m] is the 1-D SPIO density, $\mathcal{L}[\bullet]$ is the Langevin equation, and H_{sat} [A/m] measures how easily a SPIO saturates. If we specify $H(x, t) = G(x - x_s(t))$ where G [A/m^2] is the magnetic field gradient and $x_s(t)$ [m] is the position of the FFP (i.e., $x_s(t)=-H_{\text{homogeneous}}(t)/G$), then the adiabatic signal can be computed via the reciprocity theorem (see [25])

$$s_{\text{adiab}}(t)=-\frac{d}{dt}\int\int\int B_1 M_{\text{adiab}}(x,t)dxdydz \quad (2)$$

$$=\dot{x}_s(t)\gamma\left(\rho(x)*\dot{\mathcal{L}}\left[\frac{Gx}{H_{\text{sat}}}\right]\right)| \quad (3)$$

where B_1 [T/A] is the sensitivity of the receive coil. Here, we defined the scalar terms $\gamma\triangleq B_1 mG/H_{\text{sat}}$. Note that MPI signal is a spatial convolution evaluated at the instantaneous FFP location multiplied by the instantaneous FFP velocity $\dot{x}_s(t)$ [m/s].

We now derive the adiabatic *X-Space Image Reconstruction Equation* by simply dividing the received signal by the instantaneous FFP velocity and scalar terms γ to obtain

$$\hat{\rho}_{\text{adiab}}(x_s(t))=\frac{s_{\text{adiab}}(t)}{\dot{\gamma}x_s(t)} \quad (4)$$

where $\hat{\rho}_{\text{adiab}}(x_s(t))$ is the adiabatic x-space image. Computing (4), we obtain the *Adiabatic X-Space Imaging Equation*:

$$\hat{\rho}_{\text{adiab}}(x_s(t))=\rho(x)*h(x)\big|_{x=x_s(t)} \quad (5)$$

which is the 1-D magnetic particle distribution convolved with the MPI 1-D point spread function (PSF), which we can clearly identify from this equation to be the derivative of the Langevin equation: $h(x) = \dot{\mathcal{L}}[Gx/H_{\text{sat}}]$.

The x-space analysis describes MPI as sampling of a linear, space-invariant (LSI) system, with an input of the SPIO spatial distribution and an output of the native image of that SPIO distribution. The x-space image reconstruction algorithm is quick, robust, and produces no noise gain. The x-space theory was derived with three physical assumptions [11], [12].

1. The instantaneous FFP location is uniquely defined at every point in time. The unique FFP is guaranteed provided that the homogeneity of the gradient field and the FFP shifting field are adequately uniform over the imaging field-of-view (FOV). Even modest tolerances (about 20%) guarantee a unique FFP for 3-D imaging MPI scanners.
2. First harmonic (the fundamental tone) information, which must be filtered out to avoid direct feedthrough contamination, is completely recoverable. Experimental proof that this lost first harmonic information is retrievable can be found in [12], [13], [26].

3. Rotation and alignment of the net magnetization of the SPIOs is adiabatic, or instantaneous, with the applied magnetic field. This assumption is not strictly valid. There have been studies on relaxation in MPI [22], [27] but to date no one has studied the effect of relaxation on image reconstruction or resolution.

B. Non-Adiabatic X-Space Theory in One Dimension

The well-established literature on ferrofluids typically models magnetic nanoparticle relaxation as a first-order Debye process. Hence, we adopted their first-order model to see if this model could predict our experimental findings in x-space MPI. One component of the Debye model is given by the differential equation [14], [15]

$$\frac{dM(x,t)}{dt} = -\frac{(M(x,t) - M_{\text{adiab}}(x,t))}{\tau} \quad (6)$$

where $M_{\text{adiab}}(x, t)$ [A/m] is the adiabatic magnetization, $M(x, t)$ [A/m] is the non-adiabatic magnetization, and τ [s] is the relaxation time constant. Solving this differential equation is straight forward, and one obtains this *temporal* convolution

$$M(x,t) = M_{\text{adiab}}(x,t) * \frac{1}{\tau}\exp(-t/\tau)u(t) \quad (7)$$

for $\tau > 0$ where $u(t)$ is the Heaviside function. This result shows that SPIO magnetization can be approximated as a *temporal* convolution between an exponential relaxation term and the adiabatic magnetization. We can describe magnetization in a more general sense as a temporal convolution between the adiabatic magnetization and a convolution kernel $r(t)$ which represents the relaxation process

$$M(x,t) = M_{\text{adiab}}(x,t) * r(t). \quad (8)$$

In this work, because we assume a Debye relaxation process, the relaxation term is an exponential decay, $r(t) = (1/\tau)\exp(-t/\tau)u(t)$. A common alternative would be a relaxation process modeled as a Gaussian decay. Additionally, the relaxation time constant, τ, could vary with nanoparticle size or other parameters, and there is always a distribution of nanoparticle sizes in any voxel. Hence, $r(t)$ could represent the sum of all the particles' relaxation processes; however in this work we use a single relaxation time constant τ. In any of these cases, the relaxation convolution breaks the adiabatic assumption made in the original x-space theory of MPI.

We combine (1) and (8) to obtain

$$M(x,t) = m\rho(x)\delta(y)\delta(z)\mathcal{L}\left[\frac{H(x,t)}{H_{\text{sat}}}\right] * r(t) \quad (9)$$

as the full expression for non-adiabatic magnetization. To calculate the signal received by an inductive pick-up coil, we again use the principle of reciprocity. Evaluating the derivative using the convolution differentiation property $d(f * g)/dt = (df/dt) * g = f * (dg/dt)$ [28], we find that the resulting signal equation is a temporal convolution between the adiabatic signal and the relaxation convolution kernel

$$s(t) = s_{\text{adiab}}(t) * r(t) \quad (10)$$

$$= \left(\dot{x}_s(t) \gamma \rho(x) * h(x) \big|_{x=x_s(t)} \right) * r(t). \quad (11)$$

Note that the first operation is a *spatial* convolution, whereas the second operation is a *temporal* convolution. Both convolutions can contribute to spatial blur in the reconstructed MPI image. However, they manifest very differently.

To reconstruct, we perform velocity compensation and gridding as performed in (4). However, in this case velocity compensation imposes a challenge because now we cannot simply divide the signal by the FFP velocity. Therefore, the non-adiabatic image reconstruction requires a modification. Because relaxation temporally delays the received signal, we estimate that the peak signal is delayed by approximately half the relaxation time. Therefore, we modify the *Non-Adiabatic X-Space Image Reconstruction Equation* to read

$$\widehat{\rho}(x_s(t)) = \frac{s(t)}{\gamma \dot{x}_s(t - \frac{\tau}{2})}. \quad (12)$$

Here, we perform velocity compensation with the FFP velocity temporally delayed by half the relaxation time. Below we show that this approximation performs well in both simulations and experiments. The resulting image is approximated by the *Non-Adiabatic X-Space Imaging Equation*

$$\widehat{\rho}(x_s(t)) \approx \left(\rho(x) * h(x) \big|_{x=x_s(t)} \right) * r(t). \quad (13)$$

Again, we note this equation represents the SPIO density *spatially* convolved with the adiabatic PSF (the derivative of the Langevin equation), and now additionally *temporally* convolved with the relaxation term. Both convolutions blur the SPIO magnetization density, so both are critical to understanding and improving resolution and signal.

In Fig. 1, we see that the addition of relaxation effects into the x-space theory causes an *asymmetric blur* based on scanning direction. With a sinusoidal excitation field, the FFP oscillates back and forth in the *positive* and *negative* directions. With relaxation included, there is a visible alternation in the blur on alternating scanning directions. This asymmetry differs qualitatively from the adiabatic formulation in which the blur is completely symmetric regardless of scanning direction.

III. Methods

A. Berkeley X-Space Projection MPI Scanner

The Berkeley x-space projection MPI scanner used to acquire images in this study scans with a FFL instead of a FFP [Fig. 2(a)]. The scanner has a 2.3 T/m main field gradient and a sinusoidal excitation field operating at 22.9 kHz. Phase calibration was performed by using an SPIO sample (50 nm hydrodynamic diameter fluidMAG nanoparticles by Chemicell, Berlin, Germany) which experimentally demonstrated a negligible relaxation time. For more details on the Berkeley FFL scanner, refer to [8], [12]. For scanning, we laser cut an acrylic line resolution phantom with wells of 1.74 ± 0.10 mm thickness, as measured by micrometer (Fig. 4). The three pairs of wells were spaced 7.96 ± 0.07 mm, 5.95 ± 0.08 mm, and 3.93 ± 0.19 mm apart, as measured by micrometer from center to center of the wells. These wells were filled with 20-fold diluted Resovist particles (20 μM iron, Bayer-Schering, Berlin, Germany), a commercially-manufactured SPIO tracer developed for MRI [29].

B. Berkeley X-Space Relaxometer

The Berkeley MPI relaxometer [Fig. 2(b) and (c)] measures the x-space PSF without an imaging gradient [11], [30]. This system has an analogous goal as the MPI spectrometer, which is tailored to harmonic reconstruction methods [31], [32]. Unlike the spectrometer, this device measures information solely in the time domain, so it is suitable for the x-space reconstruction method. The system has an excitation electromagnet and a bias coil. Varying the bias field enables us to simulate moving a point source sample in a gradient field. The virtual FFP is scanned using a resonant excitation coil, and the signal is received by an inductive receiver coil.

The bias coil is driven by an audio amplifier (AE Techron LVC5050, Elkhart, IN) at bias fields up to ± 180 mT. The excitation coil generates a sinusoidal magnetic field of 10–200 mT-pp strength at frequencies ranging from 1.5 to 11.5 kHz and is driven by an audio amplifier (AE Techron LVC5050, Elkhart, IN). The signal is received using a gradiometric receive coil and is digitized by a 12-bit data acquisition system at 10 MSPS (National Instruments PCI-6115, Austin, TX). Custom software written in MATLAB (Mathworks MATLAB, Natick, MA) controls the system. We performed phase matching using an inductive pick-up coil and by further calibrating phase with a SPIO sample (50 nm hydrodynamic diameter fluidMAG nanoparticles by Chemicell, Berlin, Germany), which had negligible relaxation times. We measured the PSFs of Resovist particles (Bayer-Schering, Berlin, Germany) in the relaxometer.

Here, the partial FOV method was employed, similar in goal to the focus-field methodology of Philips [33]–[35], but with some crucial distinctions in implementation, as detailed in [12], [13], [26]. Numerous overlapping partial FOVs are employed to cover a full FOV. The excitation field strength determines the size of each partial FOV. A homogeneous dc field is progressively adjusted to offset the partial FOV center points, ensuring overlap between partial FOVs. This allows for reconstructing a much wider spatial FOV. During reconstruction these partial FOVs are stitched together to create the full PSF. Because we lose the first harmonic content of the MPI signal, we perform a dc recovery algorithm during this reconstruction [12], [13], [26].

C. Theoretical Calculations

Theoretical x-space signals were computed using MATLAB software (Mathworks MATLAB, Natick, MA). The adiabatic x-space theoretical signal was calculated using (2), and the non-adiabatic x-space theoretical signal was calculated using (10) with an exponential decay term for the convolution kernel $\dot{r}(t)$. A log normal distribution of SPIO diameters was used to calculate the H_{sat} and m variables in $s_{adiab}(t)$. The relaxation term $\dot{r}(t)$ was calculated based on a relaxation time parameter τ. Although the relaxation time could be calculated based on a theoretical prediction of τ, which often depends on the distribution of SPIO diameters, we used a single time constant, which we estimated by data fitting, as described in Section III-D. The theoretical signal response for 10 cycles of the excitation field was sampled at a rate corresponding to an analog sampling rate of 2 MHz, which is adequate to capture relaxation times approaching a microsecond. The excitation field was chosen as a sinusoid with the frequency and field strength of the relaxometer (Section III-B). Signal responses for the positive and negative scanning directions were separated based on whether the FFP velocity was positive or negative.

D. Fitting Algorithm for Relaxation Time Measurements

The experimental relaxometer signals were fit using a nonlinear least-squares optimization method that assumes a log normal particle size distribution and a single relaxation time constant. The fitting algorithm calculates theoretical signals, as described in Section III-C,

for each candidate particle size distribution and relaxation time. All fitting algorithms were performed using only the theoretical and experimental signals in the positive scanning direction. The experimental signal was acquired with a single FOV in the Berkeley x-space relaxometer. The best estimate of the nanoparticle relaxation time τ was solved by minimizing the error between the data and the theory. Good correspondence between this method's fitted SPIO diameter distribution and with size measurements using transmission electron microscopy was previously shown in [30].

IV. Results

A. Relaxation Blurs the X-Space Image in the Scanning Direction

We calculated MPI point spread functions according to both the adiabatic and non-adiabatic x-space theories [(2) and (10), respectively] for two experimental scenarios, one in the Berkeley x-space projection MPI scanner [Fig. 3(a) and (b)] and the other in the Berkeley x-space relaxometer [Fig. 3(c) and (d)]. All theoretical PSFs were normalized with the adiabatic theoretical signal. Comparing the non-adiabatic signals to the adiabatic signals, relaxation in the non-adiabatic x-space theory caused a loss in SNR of the signal and caused an asymmetric blur in the scanning direction of the image. This blur spatially shifts the peak signal in the image and increases the PSF's full-width at half-maximum (FWHM), which we use to define our MPI resolution [36]. As these image effects were seen in the scanning direction, the reconstructed theoretical images for the positive and negative scanning directions were not identical.

B. MPI X-Space Theory With Relaxation Predicts Point Spread Function

1. *Berkeley X-Space Projection MPI Scanner:* The calculated adiabatic and non-adiabatic x-space PSFs were compared with experimental PSF data obtained for Resovist particles in the projection MPI scanner. For the non-adiabatic theory, the (single) relaxation time constant was estimated from a single-FOV PSF of Resovist measured in the relaxometer under equivalent scanning conditions. These theoretical signals were compared to a 1-D profile through a scanner image of an amount of undiluted Resovist (2 μL), small enough to act as a point source [Fig. 3(a) and (b)]. Both the experiment and the theory are illustrated for the positive scanning direction only. Both theoretical signals were normalized with the adiabatic theoretical signal, and the experimental signal was normalized with the non-adiabatic theoretical signal for illustration purposes. The adiabatic x-space theory predicted the PSF to have a FWHM of 2.0 mm, whereas the non-adiabatic x-space theory predicted a FWHM of 3.1 mm. The experimental PSF of the scanner image had a FWHM measurement nearly identical to that of the non-adiabatic theory, 3.1 mm.
2. *Berkeley X-Space Relaxometer:* We also calculated the adiabatic and non-adiabatic x-space theoretical PSFs using the same scanning parameters as a relaxometer measured PSF for Resovist particles [Fig. 3(c) and (d)]. To calculate the non-adiabatic theoretical PSF, we used a relaxation time constant which was measured under identical scanning conditions (see Section III-D). Both theoretical PSFs were normalized with the adiabatic theoretical PSF. The experimental PSF was then normalized with the non-adiabatic theoretical PSF for illustration purposes. The adiabatic theoretical signal predicted the FWHM of the PSF to be 4.8 mT, whereas the non-adiabatic theory predicted a FWHM of 9.7 mT. The FWHM of the experimentally measured PSF was 10.7 mT.

C. MPI X-Space Theory With Relaxation Predicts Experimental Images

We scanned a line resolution phantom of 20-fold diluted Resovist in the Berkeley x-space projection MPI scanner and compared a 1-D profile through the center of the acquired positive velocity image to the predictions of the adiabatic and non-adiabatic x-space theories (Fig. 4). For the non-adiabatic x-space theory, we used the measured relaxation time for Resovist in the Berkeley x-space relaxometer under equivalent scanning conditions (Section III-D). We normalized the 1-D image profiles of both the theories to the experimental image profile. Scanning direction dependencies are demonstrated in the experimental profile as the right well in each well pair has a higher peak than the left well as some of the signal in the left well has been blurred to the right (the positive scanning direction). Additionally, the experimental profile is blurred much further in the positive scanning direction than the profile predicted by the adiabatic x-space theory, whereas the non-adiabatic theory shows similar widths as and excellent alignment with the experimental profile.

V. Discussion

The incorporation of Debye first-order relaxation modeling into the x-space analysis of MPI resulted in several predictions, including the following.

1. *Asymmetric, Increased Blurring*: Relaxation caused a temporal lag in SPIO response, which blurred the PSF in the scanning direction of the spatial domain after x-space reconstruction. Blurring due to relaxation caused a spatial shift in peak signal that alternates in the positive and negative directions. Relaxation also increases total blur, as measured by overall FWHM.
2. *SNR Loss*: Due to relaxation blurring, the peak MPI signal amplitude decreases since the rate of change of flux is slowed. Because the noise was unchanged, this decrease in signal becomes a loss in SNR.

Overall, the simple Debye first-order non-adiabatic x-space analysis showed excellent agreement with experimental data. The addition of relaxation effects improved agreement between the x-space theory and experimental images acquired from point sources and the more complex line resolution phantom in the Berkeley x-space projection MPI scanner. The adiabatic x-space theory consistently predicted superior spatial resolution than the obtained experimental data, whereas the non-adiabatic x-space theory consistently predicted spatial resolution consistent with the data. The non-adiabatic theoretical signal had a similar shape and FWHM compared to the experimental relaxometer signal, whereas the adiabatic theory did not accurately predict the complex shape and asymmetry of the experimental relaxometer signal. It is important to note that the measured relaxation times for the two MPI systems were quite different, resulting in different degrees of relaxation-induced blurring. We believe these differences in relaxation times are due to the differences in operating frequency of the two systems, which will be an important future subject of research in order to minimize relaxation-induced blurring.

This non-adiabatic description of x-space MPI accounts for the observed asymmetry between the positive and negative directions of scanning. Most noticeably, it explains an asymmetric blurring and associated shifting artifact which were always evident in experimental data. In a rectilinear trajectory in x-space in which every other line is scanned in the opposite direction, in the resulting image, every other line would be shifted and blurred in the opposite direction. This even/odd artifact could be mitigated by using only positive (or negative) scanning direction data in a 2-D image reconstruction. Another alternative could be to use both even and odd scanning directions and a phase recovery algorithm to create a symmetric impulse response. Despite this blurring in the scanning

direction, x-space reconstruction still produces an image, albeit with a moderate loss in resolution.

This work represents the first experimental and theoretical exploration of the effects of relaxation, which has been neglected in both system matrix reconstruction and x-space reconstruction. This enhanced knowledge of how relaxation impacts the image can enable us to minimize these negative effects. SPIO characteristics can be tailored for excellent MPI resolution by maximizing the magnetic capabilities while minimizing relaxation parameters [23], [24]. We can also explore how MPI scanning parameters affect relaxation effects so that MPI scanning sequences can be designed for optimal resolution for a given SPIO. Relaxation blurring may also be reduced with postprocessing methods. By experimentally measuring the relaxation process *in vivo*, one could deconvolve the effects of relaxation using well-known methods of image processing. Deconvolution would of course increase noise [37], implying that an optimal tradeoff could be explored. Understanding relaxation and its consequences will help us to improve MPI image quality.

The current work relies on only a single relaxation time constant, yet it seems to adequately predict experimental data. Clearly, more sophisticated relaxation models, similar to the thorough work in [22] may offer improvements. Multiple relaxation times or multiple relaxation mechanisms should certainly be explored as they may be present in the *in vivo* environment.

This direction of research holds exciting potential for future molecular and cellular imaging applications of MPI. Relaxation times may be used to monitor *in vivo* parameters, in combination with SPIOs labeled with ligands designed to alter their dominant relaxation mechanism. For example, one could imagine using MPI to monitor *in vivo* viscosity [38], perhaps with no ligand. MPI may also be used one day to visualize protein or cell binding via relaxation measurements of a SPIO labeled with a tailored ligand [39], [40]. Of course, these emerging MPI molecular and cellular imaging methods must be explored with both x-space and harmonic reconstruction schemes.

VI. Conclusion

The non-adiabatic x-space theory is the first example of a MPI system theory and reconstruction scheme that accounts for relaxation effects. The non-adiabatic x-space theory showed excellent agreement with experimentally measured signals from both the Berkeley x-space relaxometer and the Berkeley x-space projection MPI scanner. Our data indicates that relaxation modeling is crucial to modeling the MPI signal. Relaxation caused a loss in SNR and an asymmetric blurring of the image in the scanning direction. We demonstrated that a simple modification to x-space reconstruction produces robust image reconstruction. Understanding relaxation’s effect on the image will help researchers to mitigate relaxation blurring and to design SPIOs and x-space scanning methods for optimal image quality.

Acknowledgments

The authors would like to express our appreciation to A. Tamrazian for his contribution to the development of the relaxometer, J. Konkle and B. Zheng for scanner operation, and K. Lu, Dr. E. Saritas, and Dr. G. Lee for their excellent discussions.

This work was supported in part by the National Institute of Biomedical Imaging and Bioengineering under Grant 1R01EB013689, in part by the UC Discovery Grant, in part by the CIRM Tools and Technology Grant RT2-01893, in part by the National Science Foundation Graduate Research Fellowship, and in part by the Berkeley Fellowship for Graduate Study.

REFERENCES

1. Ix JH, Mercado N, Shlipak MG, Lemos P, Boersma E, Linde-boom W, O'Neill WW, Wijns W, Serruys PW. "Association of chronic kidney disease with clinical outcomes after coronary revascularization: The Arterial Revascularization Therapies Study (ARTS),". Am. Heart J. 2005; vol. 149(no. 3):512–519. [PubMed: 15864241]
2. Reddan DN. "Chronic kidney disease, mortality, and treatment strategies among patients with clinically significant coronary artery disease,". J. Am. Soc. Nephrol. 2003; vol. 14(no. 9):2373–2380. [PubMed: 12937316]
3. Coresh J, Selvin E, Stevens LA, Manzi J, Kusek JW, Eggers P, Van Lente F, Levey AS. "Prevalence of chronic kidney disease the United States,". J. Am. Med. Assoc. 2007; vol. 298(no. 17):2038–2047.
4. Ferrucci JT, Stark DD. "Iron oxide-enhanced MR imaging the liver and spleen: Review of the first 5 years,". Am. J. Roentgenol. 1990; vol. 155(no. 5):943–950. [PubMed: 2120963]
5. Weissleder R, Stark DD, Engelstad BL, Bacon BR, Compton CC, White DL, Jacobs P, Lewis J. "Superparamagnetic iron oxide: Pharmacokinetics and toxicity,". Am. J. Roentgenol. 1989; vol. 152(no. 1):167–173. [PubMed: 2783272]
6. Neuwelt EA, Hamilton BE, Varallyay CG, Rooney WR, Edelman PM, Jacobs PM, Watnick SG. "Ultrasmall superparamagnetic iron oxides (USPIOs): A future alternative magnetic resonance (contrast agent for patients at risk for nephrogenic systemic fibrosis (NSF)?,". Kidney Int. 2009; vol. 75(no. 5):465–474. [PubMed: 18843256]
7. Lu M, Cohen MH, Rieves S, Pazdur R. "FDA report: Ferumoxytol for intravenous iron therapy in adult patients with chronic kidney disease,". Am. J. Hematol. 2010; vol. 85(no. 5):315–319. [PubMed: 20201089]
8. Goodwill PW, Konkle JJ, Zheng B, Saritas EU, Conolly SM. "Projection X-space magnetic particle imaging,". IEEE Trans. Med. Imag. May; 2012 vol. 31(no. 5):1076–1085.
9. Gleich B, Weizenecker J. "Tomographic imaging using the nonlinear response of magnetic particles,". Nature. 2005; vol. 435(no. 7046):1214–1217. [PubMed: 15988521]
10. Rahmer J, Weizenecker J, Gleich B, Borgert J. "Signal encoding in magnetic particle imaging: Properties of the system function,". BMC Med. Imag. 2009; vol. 9(no. 1):4.
11. Goodwill PW, Conolly SM. "The x-space formulation of the magnetic particle imaging process: 1-D signal, resolution, bandwidth, SNR, SAR, and magnetostimulation,". IEEE Trans. Med. Imag. Nov; 2010 vol. 29(no. 11):1851–1859.
12. Goodwill PW, Conolly SM. "Multidimensional x-space magnetic particle imaging,". IEEE Trans. Med. Imag. Sep; 2011 vol. 30(no. 9):1581–1590.
13. Goodwill PW, Lu K, Zheng B, Conolly SM. "An x-space magnetic particle imaging scanner,". Rev. Sci. Instrum. 2012; vol. 83:033708. [PubMed: 22462930]
14. Debye, P. Polar Molecules. New York: Chemical Catalog; 1929.
15. Shliomis MI. "Magnetic fluids,". Soviet Physics-Uspekhi. 1974; vol. 17(no. 2):153–169.
16. Brown WF. "Thermal fluctuations of a single-domain particle,". Phys. Rev. 1963; vol. 130(no. 5): 1677–1686.
17. Coffey WT, Crothers DSF, Kalmykov YP, Waldron JT. "Constant-magnetic-field effect in Néel relaxation of single-domain ferromagnetic particles,". Phys. Rev. B. 1995; vol. 51(no. 22):15947–15956.
18. Engel A, Reimann P. "Thermal ratchet effects in ferrofluids,". Phys. Rev. E. 2004; vol. 70(no. 5): 051107.
19. Felderhof BU, Jones RB. "Nonlinear response of a dipolar system with rotational diffusion to an oscillating field,". J. Phys.: Condensed Matter. 2003; vol. 15(no. 5):S1363.
20. Rosensweig RE. "Magnetic fluids,". Annu. Rev. Fluid Mechan. 1987; vol. 19(no. 1):437–461.
21. Sanchez JH, Rinaldi C. "Rotational Brownian dynamics simulations of non-interacting magnetized ellipsoidal particles in dc and ac magnetic fields,". J. Magnetism Magn. Mater. 2009; vol. 321:2985–2991.
22. Weizenecker J, Gleich B, Rahmer J, Borgert J. "Particle dynamics of mono-domain particles in magnetic particle imaging,". Proc. 1st Int. Workshop Magnetic Particle Imag. 2010:3–15.

23. Ferguson RM, Minard KR, Khandhar AP, Krishnan KM. “Optimizing magnetite nanoparticles for mass sensitivity in magnetic particle imaging,”. Med. Phys. 2011; vol. 38(no. 3):1619. [PubMed: 21520874]
24. Ferguson RM, Minard KR, Krishnan KM. “Optimization of nanoparticle core size for magnetic particle imaging,”. J. Magnetism Magn. Mater. 2009; vol. 321(no. 10):1548–1551.
25. Hoult DI, Richards RE. “The signal-to-noise ratio of the nuclear magnetic resonance experiment,”. J. Magn. Reson. 1976; vol. 24:71–85.
26. Lu K, Goodwill P, Zheng B, Conolly S. “The impact of filtering direct-feedthrough on the x-space theory of magnetic particle imaging,”. Proc. SPIE. 2011; vol. 7965:79652I.
27. Rauwerdink AM, Weaver JB. “Harmonic phase angle as a concentration-independent measure of nanoparticle dynamics,”. Med. Phys. 2010; vol. 37(no. 6):2587. [PubMed: 20632570]
28. Bracewell, RN. The Fourier Transform and Its Applications. 3rd. New York: McGraw-Hill; 2000.
29. Reimer P. “Ferucarbotran (Resovist): A new clinically approved RESspecific contrast agent for contrast-enhanced MRI of the liver: Properties, clinical development, and applications,”. Eur. Radiol. 2003; vol. 13(no. 6):1266–1276. [PubMed: 12764641]
30. Goodwill PW, Tamrazian A, Croft LR, Lu CD, Johnson EM, Pidaparthi R, Ferguson RM, Khandhar AP, Krishnan KM, Conolly SM. “Ferrohydrodynamic relaxometry for magnetic particle imaging,”. Appl. Phys. Lett. 2011; vol. 98(no. 26):262502.
31. Biederer S, Knopp T, Sattel TF, Lüdtke-Buzug K, Gleich B, Weizenecker J, Borgert J, Buzug TM. “Magnetization response spectroscopy of superparamagnetic nanoparticles for magnetic particle imaging,”. J. Phys. D: Appl. Phys. Oct.2009 vol. 42(no. 20):205007.
32. Biederer S, Sattel TF, Knopp T, LaConte L, Gleich B, Weize-necker J, Borgert J, Buzug TM. “A spectrometer for magnetic particle imaging,”. 4th Eur. Conf. Int. Fed. Med. Biol. Eng. 2009:2313–2316.
33. Gleich B, Weizenecker J, Timminger H, Bontus C, Schmale I, Rahmer J, Schmidt J, Kanzenbach J, Borgert J. “Fast MPI demonstrator with enlarged field of view,”. Proc. Int. Soc. Magn. Reson. Med. 2010; vol. 18:218.
34. Rahmer J, Gleich B, Bontus C, Schmale I, Schmidt J, Kanzenbach J, Woywode O, Weizenecker J, Borgert J. “Rapid 3-D in vivo magnetic particle imaging with a large field of view,”. Proc. Int. Soc. Magn. Reson. Med. 2011; vol. 19:3285.
35. Schmale I, Rahmer J, Gleich B, Kanzenbach J, Schmidt JD, Bontus C, Borgert J, Woywode O. “First phantom and in vivo MPI images with an extended field of view,”. Proc. SPIE. 2011; vol. 7965:796510.
36. Houston W. “The fine structure and the wave-length of the balmer lines,”. Astrophys. J. 1926; vol. 64:81.
37. Shahram M. “Imaging below the diffraction limit: A statistical analysis,”. IEEE Trans. Image Process. May; 2004 vol. 13(no. 5):677–689. [PubMed: 15376599]
38. Rauwerdink AM, Weaver JB. “Viscous effects on nanoparticle magnetization harmonics,”. J. Magnetism Magn. Mater. 2010; vol. 322(no. 6):609–613.
39. Kötitz R, Weitschies W, Trahms L, Brewer W, Semmler W. “Determination of the binding reaction between avidin and biotin by relaxation measurements of magnetic nanoparticles,”. J. Magnetism Magn. Mater. 1999; vol. 194:62–68.
40. Rauwerdink AM, Weaver JB. “Measurement of molecular binding using the Brownian motion of magnetic nanoparticle probes,”. Appl. Phys. Lett. 2010; vol. 96(no. 3):033702.

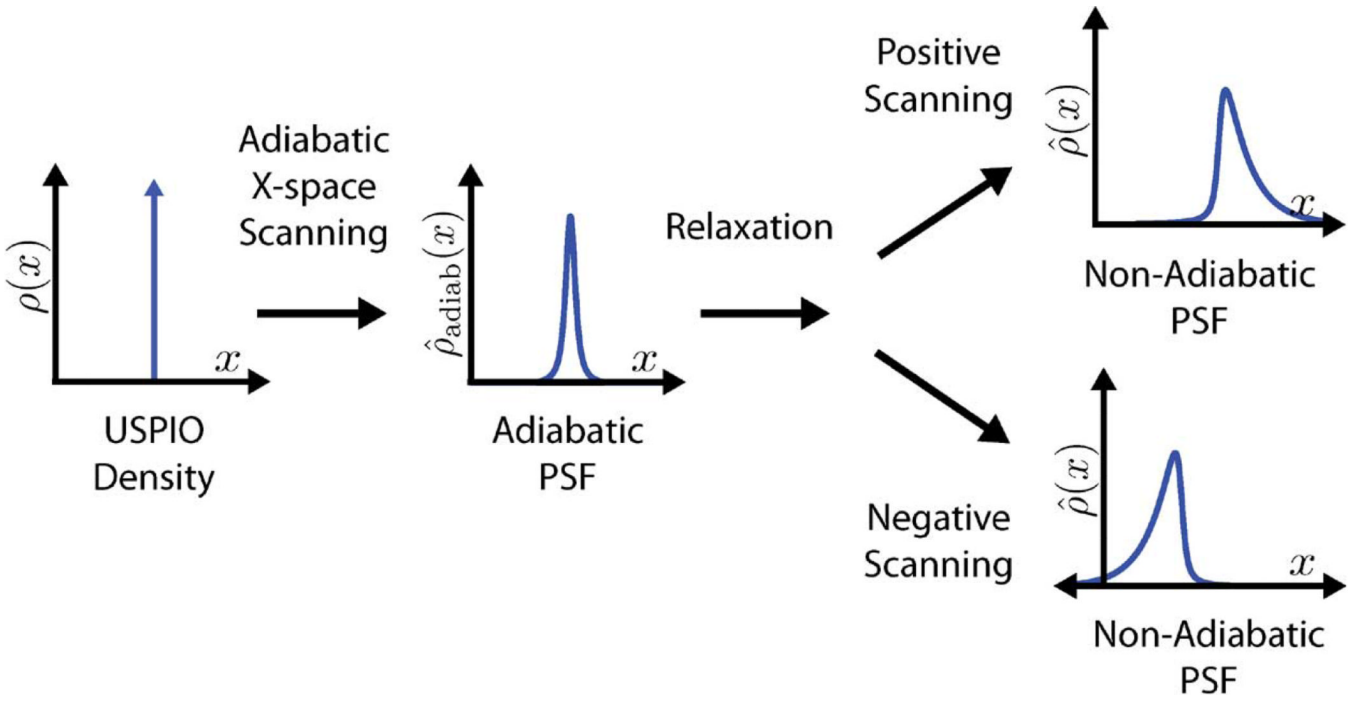

Fig. 1.

Adiabatic x-space scanning blurs the SPIO density input according to the Langevin magnetization of the SPIOs. Relaxation effects further blur the image and create an asymmetrical shape to the PSF. This blurring effect occurs in the scanning direction, which results in nonidentical PSFs for the two scanning directions.

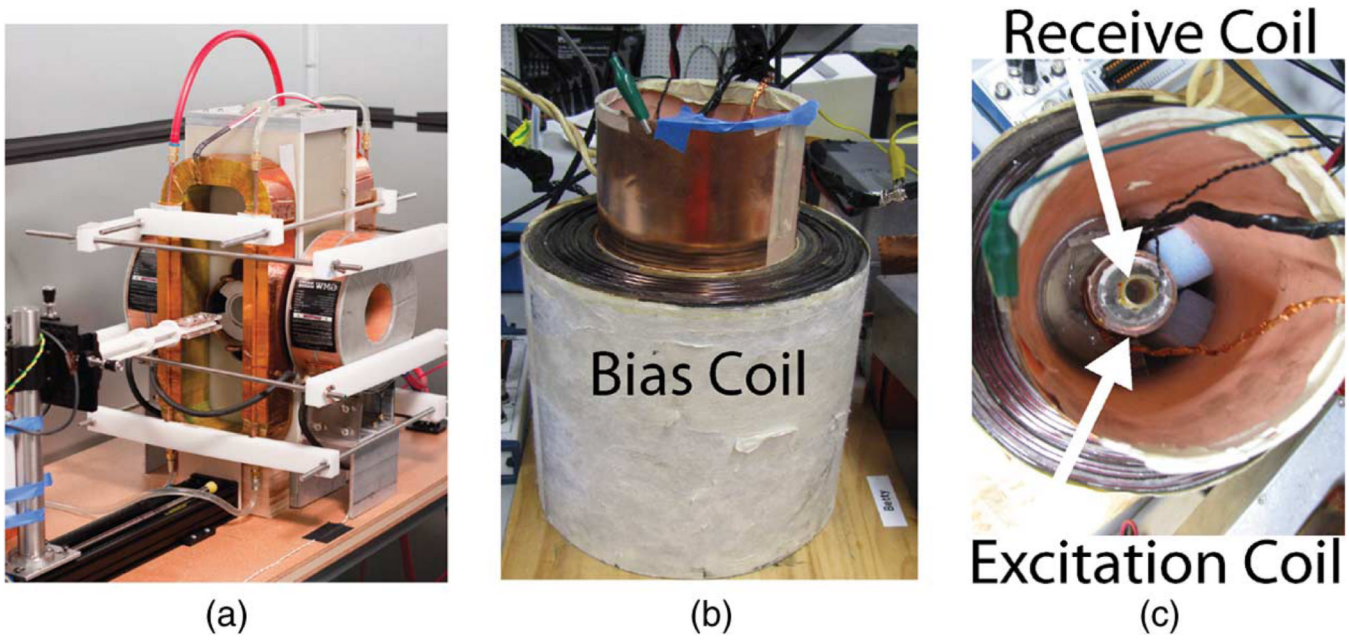

Fig. 2.

Berkeley x-space projection MPI scanner (a) acquires 2-D images. A 2.3 T/m magnetic gradient creates a FFL, and the excitation coil scans this FFL at 22.9 kHz with field strengths up to 35 mT-pp. The Berkeley x-space relaxometer, shown with side (b) and top (c) views, measures the point spread function of a particle sample. The excitation coil generates a sinusoidal magnetic field of 10–200 mT-pp strength at frequencies of 1.5–11.5 kHz. The signal received from the gradiometric receive coil is digitized at 10 MSPS without filtering. The bias coil can add ± 180 mT field for partial FOV scanning.

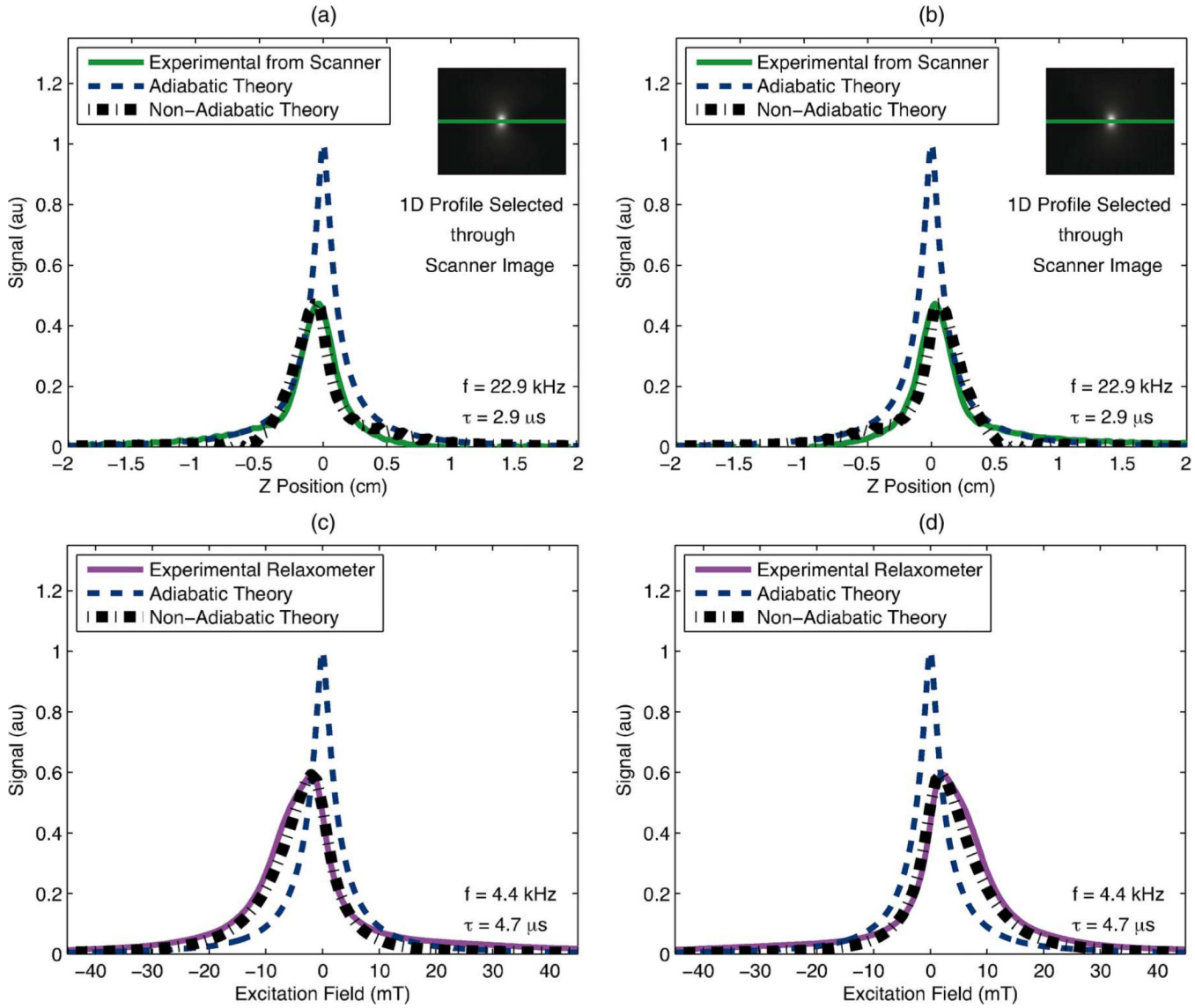

Fig. 3.

Experimentally measured PSFs displayed alongside theoretical PSFs calculated from the adiabatic and the non-adiabatic x-space theories for each scanning direction. The inclusion of relaxation into the theory predicted a significant loss in predicted resolution and peak signal and produced a shape which more closely resembled that of the experimental signal. (a), (b): We compared the x-space theoretical PSFs to a 1-D profile through (inset) a positive-velocity scan image of 2 μL of undiluted Resovist acquired in the Berkeley x-space projection MPI scanner with an excitation field of 20 mT-pp at 22.9 kHz. Scan time was 37 s and FOV was 6.6 cm × 5 cm. Non-adiabatic calculations used a measured time constant of 2.9 μs. (c), (d): We measured a PSF of Resovist in the Berkeley x-space relaxometer with an excitation field of 60 mT-pp at 4.4 kHz. Non-adiabatic calculations used a measured time constant of 4.7. (a) Resovist in scanner: negative scanning. (b) Resovist in scanner: positive scanning. (c) Resovist in relaxometer: negative scanning. (d) Resovist in relaxometer: positive scanning.

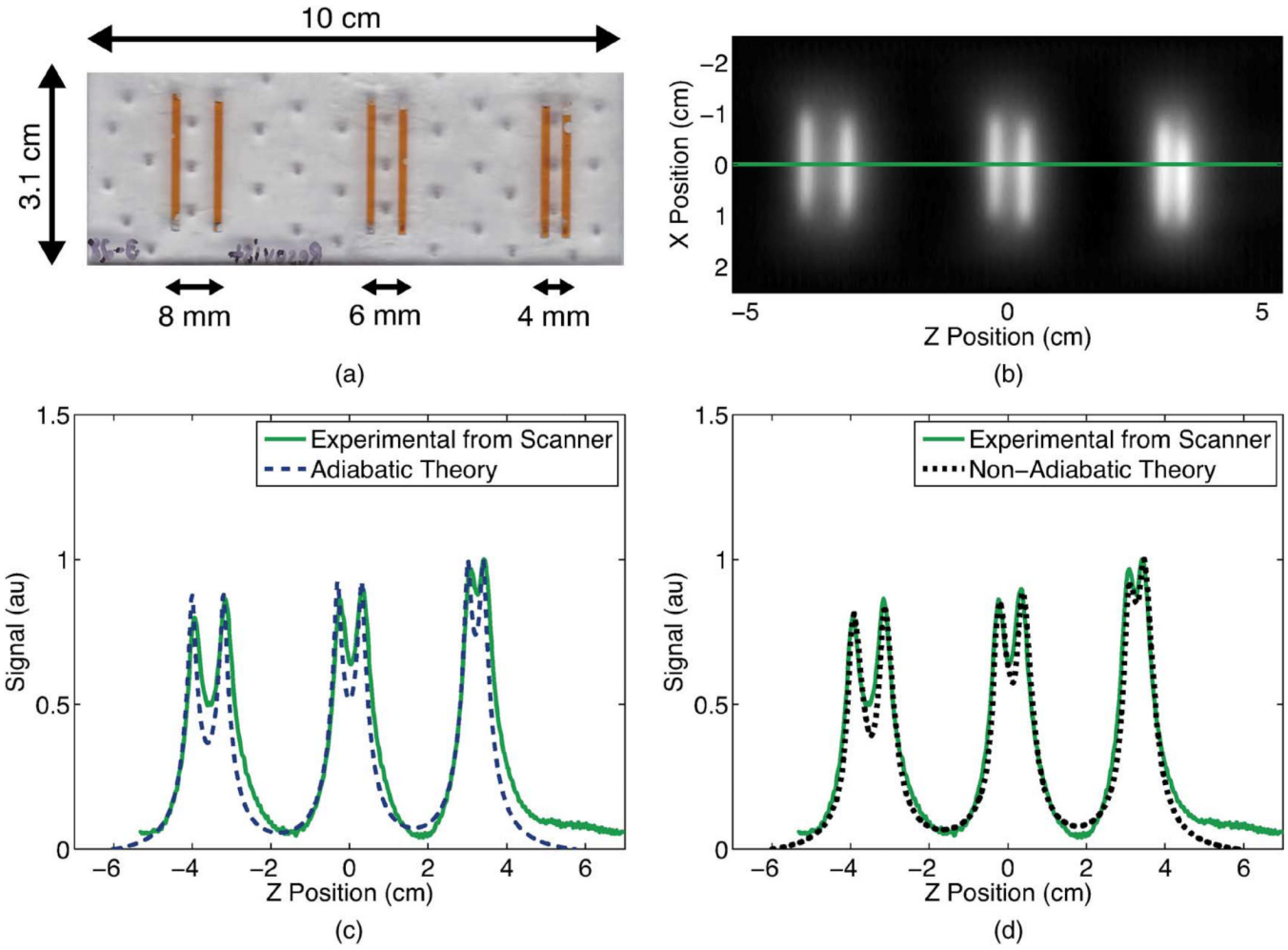

Fig. 4.

A line resolution phantom (a) was constructed with 1.75-mm-wide wells which were filled with 20 × diluted Resovist. We acquired a positive-velocity scan image (b) of this phantom in the Berkeley x-space projection MPI scanner at 20 mT-pp for a scan time of 59 s and a FOV of 13 cm 5 cm. No deconvolution was performed. We visualized a 1-D profile through the center of this image and compared this profile to the image predicted by the adiabatic x-space theory (c) and by the non-adiabatic x-space theory (d). The experimentally measured image showed better agreement with the non-adiabatic x-space theory than with the adiabatic x-space theory. Non-adiabatic calculations used a measured relaxation time constant of 2.9 μs.